Journal of the Optical Society of Korea
Vol. 20, No. 5, October 2016, pp. 593-600

ISSN: 1226-4776(Print) / ISSN: 2093-6885(Online)
DOI: http://dx.doi.org/10.3807/JOSK.2016.20.5.593

Cooling Geometry Dependent Operation Properties in a Diode End-Pumped Monolithic Yb:YAG Laser

Hee-Jong Moon[1]* and Changhwan Lim[2]

[1]*Department of Optical Engineering, Sejong University, Seoul 05006, Korea*
[2]*Quantum Optics Division, Korea Atomic Energy Research Institute, Daejeon 34057, Korea*

(Received May 12, 2016 : revised August 5, 2016 : accepted August 17, 2016)

Operation properties, such as output power, beam radius, and crystal temperature rise were investigated in a diode-pumped edge-cooled monolithic Yb:YAG laser with ~ 4 W pumping level. The output power showed saturation behavior because of severe temperature rise and poor spatial overlapping between pump beam and lasing mode. Face cooling geometry by using a sapphire plate was also investigated. No apparent saturation behavior in output power was observed due to the reduced temperature rise, which could be attributed to efficient heat removal through the crystal-sapphire interface.

Keywords : Yb:YAG, Temperature Rise, Peak Shift, Plane Stress Approximation
OCIS codes : (140.3615) Lasers, ytterbium; (140.3480) Lasers, diode-pumped; (140.6810) Thermal effects

I. INTRODUCTION

Yb:YAG crystals have been widely studied because they have various advantages for efficient diode-pumped lasers [1-4]. Yb:YAG has a broad pump line at 940 nm that is 10 times broader than the 808 nm pump line in the conventional Nd:YAG, which makes the system less sensitive to thermal drift of the laser diode (LD) wavelength [5]. Due to high quantum efficiency of the 1048 nm transition line, the thermal load can be substantially reduced compared to that of the Nd:YAG lasers. Because the doping concentration of Yb^{3+} can exceed 50 %, the optimal crystal thickness for diode end pumping can be fairly shortened to below a few 100 μm, which is beneficial for thin disk type or monolithic lasers [6, 7]. Due to relatively broad gain bandwidth, mode locking operations for ultrashort pulse lasers are also reported [8, 9].

Due to the quasi-three level nature of Yb^{3+}, the operation properties of the Yb:YAG laser depends strongly on the crystal temperature. At room temperature, the low level of 1048 nm laser transitions line has a population of ~ 0.02, which induces non-negligible reabsorption loss [10]. Because the reabsorption loss tends to increase with temperature, the crystal temperature rise due to the thermal load might degrade the laser performance such as the laser efficiency. Therefore, some cooling scheme is essential to prevent severe crystal temperature rise by the absorbed pump beam. A proper measurement scheme for crystal temperature rise is also required to evaluate the cooling capacity.

A few noncontact measurement schemes for crystal temperature have been reported, such as crystal surface temperature mapping by using an infrared camera and the spectral analysis of the upconversion emission from the crystal impurity [11, 12]. Recently, we reported an excellent measurement scheme for crystal temperature by analyzing the spectral shift of the lasing peaks [13]. The temperature and strain profiles induced by the thermal load produce phase change on the cavity modes, resulting in the red shift of each lasing peak. For a small crystal thickness where the plane stress approximation (PSA) is valid, the amount of red shift could be related linearly to the average temperature rise along the beam axis [13].

On the other hand, the previous work was limited to a low pumping level (up to ~ 1 W) with a very small pump spot size (~ 60 μm) [14]. Thus, the reported maximum temperature rise was only ~ 20℃ in an edge cooling configuration. It

*Corresponding author: hjmoon@sejong.ac.kr
Color versions of one or more of the figures in this paper are available online.

This is an Open Access article distributed under the terms of the Creative Commons Attribution Non-Commercial License (http://creativecommons.org/licenses/by-nc/3.0/) which permits unrestricted non-commercial use, distribution, and reproduction in any medium, provided the original work is properly cited.

Copyright © 2016 Optical Society of Korea

should be valuable to apply the measurement scheme to a higher pumping level because increased temperature rise might induce unexpected operation behaviors of the laser. Here, we applied the scheme to a higher (~ 4 W) pumping level to measure the temperature rise, and we investigated the laser operation properties. We also investigated the effect of the cooling geometry on the temperature rise and laser operation properties by using two PSA valid face cooling configurations.

II. EXPERIMENTS

The experimental setup for the temperature measurement scheme is shown in Fig. 1, which is similar to that in our previous paper [13]. The crystal used was the same as the previous one (20 at.% Yb:YAG with a 0.75 mm thickness). Both faces of the crystal had dichromatic coatings (input face; HR at 1050 nm and HT at 930 nm, output face; 92% reflectivity at 1050 nm and HR at 930 nm). The crystal was sandwiched by two contacting copper plates having a central hole of 3 mm diameter, as depicted in the crystal holder in Fig. 1. The crystal holder was temperature controlled in a crystal oven. A collimated fiber-coupled laser diode (FC-LD) module was used for continuous-wave (cw) pumping. The core size of the fiber (NA of 0.22) in FC-LD was 105 μm, two times larger than that of the previous one [13]. The collimated beam passed through an optical isolator consisting of a Faraday rotator and two prism polarizers (PP_1, PP_2) in order to block reflected light to FC-LD. Aspheric lenses (L_1, L_2) with the focal lengths of 18 mm were used for focusing and re-collimation of the pump beam. Finally the pump beam was focused on the crystal by lens L_3 (f_3 = 18 mm). The maximum pump power at the crystal was ~ 4.5 W with a wavelength of 930 nm.

The pump beam can be switched from cw mode to pulse mode by inserting an optical chopper between L_1 and L_2. The chopper blade, locating near the focal region of the pump beam, had a small single slot for one pumping pulse per turn. The lasing spectra in pulse mode (or cw mode) were measured by an optical spectrum analyzer (OSA). The pulse signal of a photo diode, detecting the reflected beam from the crystal through the slot, was used as the triggering input signal of the OSA in pulse mode.

III. CW OPERATIONAL PROPERTIES

The pump spot size focused by L_3 at the crystal is an important parameter on the operation performance. We measured pump beam size (or diameter) in free space by using previous knife edge method [13]. The pump beam size was defined as the distance between tail points of the pump beam profile, as described in the previous work [13]. The spot size of the pump beam was about 120 μm, which is significantly larger than the previous one of 68 μm due to the larger fiber core size. The measured beam quality factor M^2 of the focused pump beam was ~ 25. Because the size variation of the pump beam near the focal spot was very small (~ 10% in the crystal length range), the pump beam size could be approximated as a constant in the crystal. The absorption efficiency during the double pass in the crystal was measured as ~ 80 % and was insensitive to the LD current or input pump power.

Figure 2 shows the dependence of the cw laser output power P_{out} on the input pump power P_{in}. The threshold pump power was about 0.4 W. The output power increased linearly up to P_{in} ~ 2.3 W, as shown as a dotted line. The slope efficiency with respect to the absorbed power was estimated as about 43%, which is slightly smaller than the previous one [13]. When the input power exceeds 2.3 W, P_{out} was saturated at around 0.7 W and then decreased. If the input power increased more than 3.3 W, P_{out} was unstable and rapidly decreased to 0. This saturation effect of P_{out} might be due to severe temperature rise in the crystal or poor

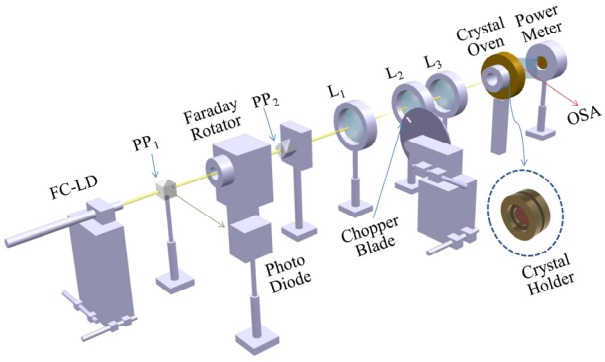

FIG. 1. Experimental setup. FC-LD: collimated fiber-coupled laser diode, PP_1 & PP_2: prism polarizers, L_1: focusing lens (f_1 = 18 mm), L_2: collimating lens (f_2 = 18 mm), L_3: focusing lens (f_3 = 18 mm).

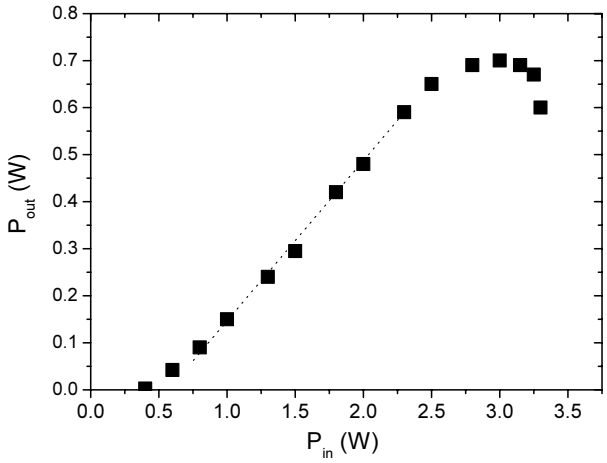

FIG. 2. Dependency of the cw laser output power P_{out} on the input pump power P_{in}.

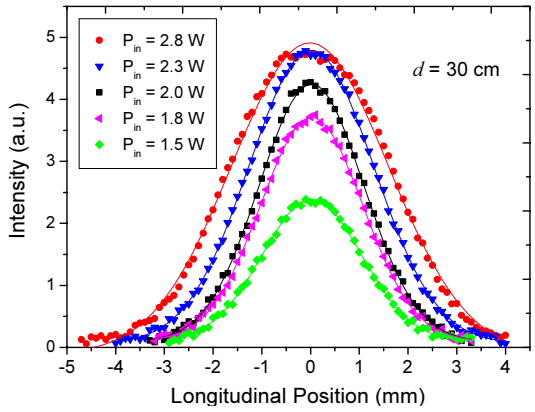

(a)

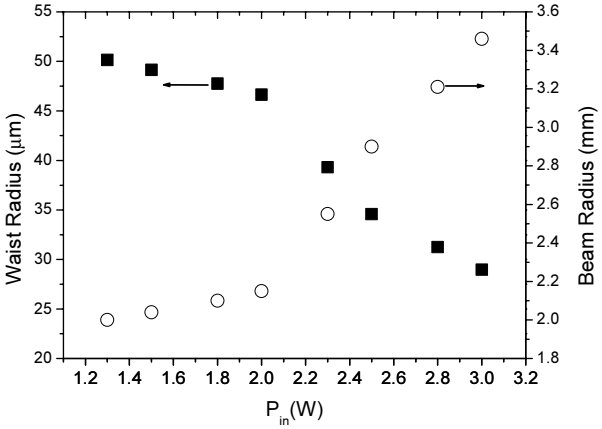

(b)

FIG. 3. (a) Pump power dependent output intensity profile measured at a distance $d = 30$ cm from the crystal. (b) Pump power dependent output beam radius fitted by Gaussian function. Corresponding waist radius of TEM_{00} mode is also shown

spatial overlapping between pump beam and lasing mode.

The intensity profile of the cw output beam was measured by a pinhole-attached photo diode (not shown in Fig. 1), as illustrated in the previous work [13]. Figure 3(a) shows the output beam profiles at various P_{in}, in which the distance d from crystal to photo diode was 30 cm. The profiles were well fitted with the Gaussian functions depicted as lines, which means that the lasing transverse mode was TEM_{00} at all ranges of P_{in}. Figure 3(b) shows the pump power dependent output beam radius $w(z = d)$. It increased slowly up to P_{in} around 2.0 ~ 2.3 W and then radically. By assuming the lasing mode was TEM_{00} or Gaussian mode, the waist radius w_0 of TEM_{00} mode in the crystal can be estimated from the relation $w_0 = \cong \frac{\lambda d}{\pi w(d)}$ [14]. In Fig. 3(b), dependency of w_0 on the pump power is also shown. Because the waist radius w_0 is inversely proportional to the beam radius $w(d)$, it decreased slowly at first and then rapidly above P_{in} ~ 2.3 W. For small P_{in} ($\leq$ 2.0 W), the waist size 2 w_0 of TEM_{00} was about 100 μm, which is slightly smaller than the measured pump spot size of ~ 120 μm. Thus, the spatial overlapping between pump beam and lasing mode should be good and resultant lasing efficiency was measured relatively high at low pump power in Fig. 2. However, the spatial overlapping became poor due to rapid decrease of w_0 when P_{in} exceeded 2.3 W, resulting in the saturation behavior of the output power, as shown in Fig. 2. At P_{in} = 3.0 W, the waist size decreased to ~ 60 μm, which is only half of the pump spot size. Thus, the saturation behavior in Fig. 2 above P_{in} ~ 2.3 W can be mainly attributed to the poor spatial overlapping between pump beam and lasing mode. The rapid decrease of w_0 should be due to the enhanced thermal lensing effect, which is a result of the severe thermal load [15].

IV. TEMPERATURE RISE & SPECTRAL SHIFT

Figure 4(a) shows the pumping and cooling configuration adapted in this study. The cooling geometry is basically the same as the previous edge cooling arrangement [13].

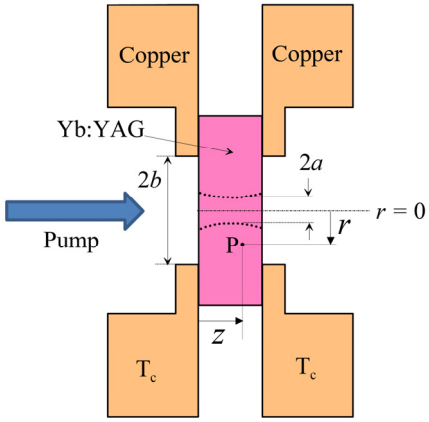

(a)

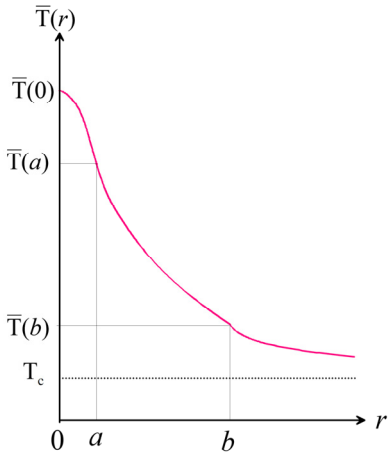

(b)

FIG. 4. (a) Schematic edge cooling geometry. (b) The expected curve of average temperature $\overline{T}(r)$.

The crystal (thickness of L) is sandwiched by copper plates with a central hole (diameter of 2*b*). The pump spot size 2*a* is negligibly smaller than 2*b*. The copper plate temperature T_c is controlled to a constant value in the crystal oven. When the crystal absorbs radially symmetric pump beam, some portion of the absorbed energy converts to heat. The fractional thermal load η, the ratio of generated heat to absorbed energy, is much smaller than 0.11 in Yb:YAG [16]. The generated heat and its radial flow through the crystal with a limited thermal conductivity enhance the crystal temperature. The local temperature profile T(*r*, *z*) at a point P in the crystal is a function of the radial distance *r* and of the longitudinal distance *z*. Calculation of T(*r*, *z*) at all points in the crystal is theoretically possible by solving the heat equation and by applying boundary conditions on the crystal-copper interface, but is very difficult under real circumstances because there are undetermined parameters such as thermal contact resistance [17]. Averaged temperature with respect to *z* around the pump beam region is an important parameter because the lasing mode experiences not the local temperature but averaged temperature during round trip in the crystal. Average temperature $\overline{T}(r)$ at a given *r* is defined as [17]

$$\overline{T}(r) \equiv \frac{1}{L}\int_0^L T(r,z)\,dz \tag{1}$$

Figure 4(b) shows the expected $\overline{T}(r)$ curve in the crystal of Fig. 4(a). The maximal value of $\overline{T}(0)$ is the average temperature along the beam axis. For a given pump power P_{in}, the difference $(\overline{T}(0)-\overline{T}(a))$ in the pumping hot region depends on the detailed pump beam profile. Whereas, the difference $(\overline{T}(a)-\overline{T}(b))$ in the hole region is independent of the pump profile because there occurs only heat transfer from the pump region to the heat sink (copper plate). Temperature gaps $(\overline{T}(r\geq b)-T_c)$ at the crystal-copper interface can exist because there might be thermal contact resistance [17]. The overall temperature rise $(\overline{T}(0)-T_c)$ measures the temperature change along the beam axis after pumping. It is notable that in a typical ratio of *a*/*b* (< 0.1), $(\overline{T}(0)-\overline{T}(a))$ is very small compared to the temperature rise $(\overline{T}(0)-T_c)$, which implies that the temperature rise in the crystal is nearly independent of the detailed profile of the pump beam.

Figure 5 shows measured lasing spectra at various P_{in} in cw mode and the threshold lasing spectrum in pulse mode with T_c = 20°C. The lasing spectra consisted of periodic peaks with same mode spacing of 0.4 nm at all ranges of P_{in}. This means that the lasing peaks correspond to different longitudinal modes with the same transverse mode of TEM_{00}. Hence, it was confirmed that the assumption of TEM_{00} lasing in Fig. 3(b) is reasonable. As P_{in} increased, each lasing peak shifted to the longer wavelength side. In Fig. 5, the amount of peak shift $\Delta\lambda$ is indicated as an arrow starting from a lasing peak in pulse mode, in which the temperature rise could be approximated as 0 because the duty cycle in pulse mode was very low (< 2 %).

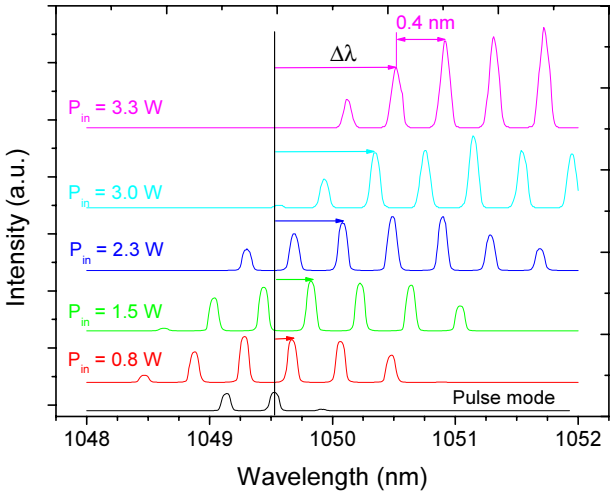

FIG. 5. Measured cw lasing spectra with P_{in} at T_c = 20°C. The threshold lasing spectrum (black line) in pulse mode is also shown. The amount of peak shift $\Delta\lambda$ in cw mode is indicated as an arrow starting from a lasing peak in pulse mode

The red shift of the lasing peak was previously attributed to the round-trip optical path length (OPL) change experienced by the cavity modes [13]. With the cw pump on, the non-uniform temperature field T(*r*, *z*) induces not only thermally induced refractive index change but also stress field in the crystal, resulting in non-uniform crystal strain field. The strain field produces crystal length change and strain induced birefringence [17]. Hence, the cavity mode experiences thermally induced refractive index change, crystal length change, and strain induced birefringence effect. For a uniform pump profile, the strain induced contribution of OPL change can be derived under the plane stress approximation (PSA), in which the axial stress approaches 0 as the aspect ratio L/2*b* decreases [18]. The used thin crystal (L/2*b* = 0.25) is in the valid regime of PSA [18]. For TEM_{00} mode, small contribution by the phase retardation effect of the Gaussian beam should also be included [14]. Because overall OPL change is positive, the cw lasing wavelength of the cavity mode will show continuous red-shift as P_{in} increases.

In the previous work, we showed that the amount of red shift $\Delta\lambda$ under PSA is proportional to the temperature rise $((\overline{T}(0)-T_c)$ as [13]

$$\Delta\lambda \cong SL_{eff}\,(\overline{T}(0)-T_c) \tag{2}$$

where SL_{eff} is the effective scale factor or ratio between $\Delta\lambda$ and the temperature rise. If the phase retardation effect is neglected, SL_{eff} ranges between SL_u and SL_{nu}, where SL_u is the scale factor in the case of uniform crystal temperature change and SL_{nu} is the scale factor in the case of non-uniform temperature and strain fields. If the temperature gap at the crystal-copper interface in Fig. 4(b) is

negligibly small, SL_{eff} approaches to SL_{nu}. Previously, we derived SL_{nu} with the material parameters and calculated in YAG crystal [13]. The calculated value of SL_{nu} was only 13 % larger than SL_u.

The phase retardation term should be accounted in a real situation where the temperature gap also exists. In the previous work with the same cooling configuration with Fig. 4(a), SL_{eff} was measured by using very complex procedure. Because the phase retardation term has a nature of decreasing the peak shift, SL_{eff} was found to be very close to SL_u [13]. Therefore, we will adapt the approximation $SL_{eff} \sim SL_u$ in this work. SL_u can be derived from the shifting behavior of a threshold lasing peak in pulse mode by varying T_c, in which the crystal temperature profile can be considered to be uniform because the non-uniformity induced by pump pulse is negligibly small. Because the temperature rise in this work is expected to be much larger than the previous case, spectral data with wide range of T_c is required. Figure 6(a) shows the linearly shifting behavior of a threshold peak in pulse mode, measured by varying T_c from 30°C to 120°C.

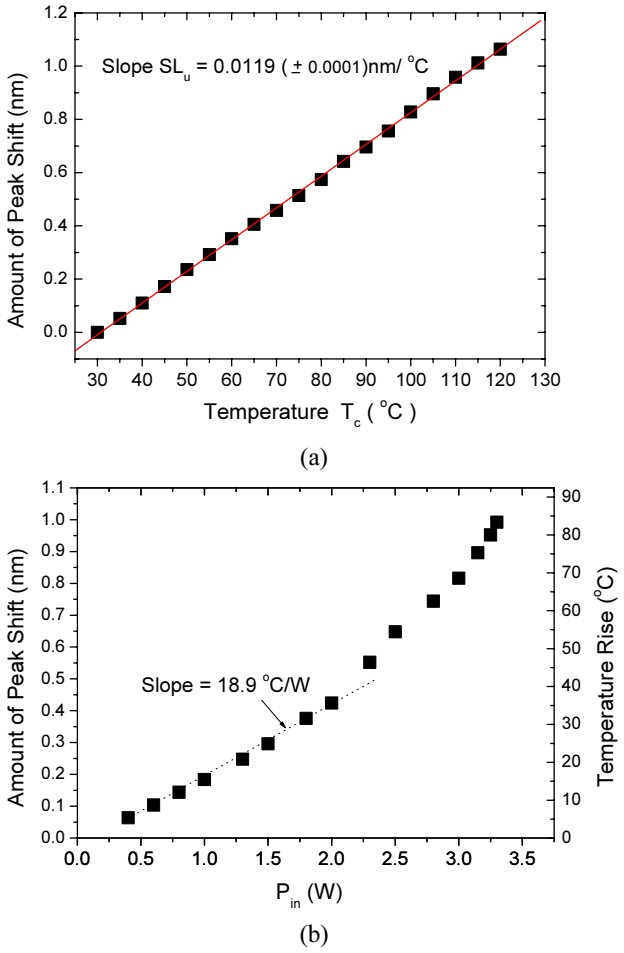

FIG. 6. (a) Relative peak shift of a threshold peak in pulse mode with T_c. The slope SL_u of the relative peak shift is fitted as 0.0119(± 0.0001) nm/°C. (b) Dependency of amount of peak shift $\Delta\lambda$ and corresponding temperature rise on P_{in}.

It shows that the slope, corresponding to SL_u, was 0.0119(± 0.0001) nm/°C.

Figure 6(b) shows the dependency of the amount of peak shift $\Delta\lambda$ measured from Fig. 5. The temperature scale, calibrated by SL_{eff} = 0.0119 nm/°C in Eq. (2), is also plotted on the right axis in order to obtain the temperature rise. The temperature rise increased linearly with a slope of 18.9°C/W as P_{in} increased up to 2.0 W. When P_{in} exceeded ~ 2.3 W, the temperature rise deviated from this trend and its slope became steeper. The deviation point of P_{in} ~ 2.3 W is coincident to those in the output power and the waist radius dependency (in Fig. 2 and 3). The temperature rise corresponding to P_{in} ~ 2.3 W was ~ 45°C (or $\overline{T}(0)$ ~ 65°C). The maximal temperature rise at P_{in} = 3.3 W was about 83°C (or $\overline{T}(0)$ = 103°C).

As the crystal temperature increases, the reabsorption loss increases, which affects laser operation performance in succession. First, the increased reabsorption loss shifts the envelope of the lasing spectrum to the longer wavelength side because the threshold condition for lasing occurs at a lower absorption region. Besides the red-shift of each lasing peak, the red-shift of lasing envelope with P_{in} can also be observable in Fig. 5. The lasing at lower absorption region which corresponds also to the lower gain region, means that the laser efficiency becomes poor, resulting in the deviation of the output power dependency, as observed in Fig. 2. Second, the fractional thermal load η under laser action depends on the laser extraction efficiency as previously reported [19]. As the laser efficiency decreases, η increases. Because the laser efficiency decreases above the deviation point, η increases (or a greater fraction of heat is generated so that steeper temperature rise occurs), which in turn degrades further the laser efficiency, resulting in the saturation of output power. Therefore, the saturation behavior can be partially attributed to increased η in addition to the poor spatial overlapping mentioned before.

In our previous case, the maximal temperature rise at P_{in} = 1.05 W was ~ 22°C. In this scaled up case, the temperature rise at P_{in} = 3.0 W, at which maximum output power was obtained, was about 68°C. Therefore, it could be concluded that the temperature rise was roughly proportional to the absorbed pump power regardless of the pump beam size, even though η and contacting condition of copper-crystal interface might be slightly different between both cases.

V. FACE COOLING GEOMETRY

The generated heat from the pump region flows radially in the edge cooling geometry of Fig. 4(a). Because the heat sink is located fairly far from the pump region, the temperature rise in the crystal was measured as high. Face cooling configuration is an efficient method of removing generated heat rapidly from the thin crystal because the heat sink can be closely contacted to the pump region [20, 21]. Figure 7 shows the face cooling configurations used

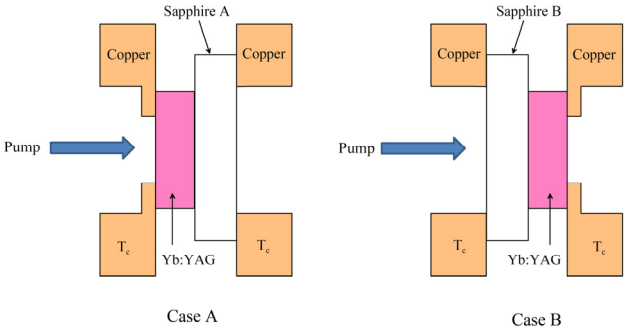

FIG. 7. Schematic face cooling geometry. Case A: Sapphire plate A is contacted to the output face of the crystal. Case B: Sapphire plate B is contacted to the input face of the crystal.

in this work, in which a sapphire plate directly contacts to one face of the crystal used in Fig. 4(a). Because the crystal was mechanically contacted to the sapphire plate with no solder, temperature gap might exist at the contact interface. This configuration is similar to the cooling setup of a thin disk laser introduced in Ref. [22, 23], in which indium-based or gold-tin solder was used for more efficient heat removal. Since additional heat flow occurs longitudinally from the pump region to the sapphire, reduced temperature rise is expected compared to the case of Fig. 4(a).

Two cases of one-face cooling were tried in this study. In case A, the sapphire A was contacted to the output face of the crystal. The non-contact side of the sapphire A was AR coated on the lasing wavelength, while the contacting side was uncoated. In case B, the sapphire B was contacted to the input face of the crystal. The contacted face of the sapphire B was uncoated, while the other side was AR coated on the pump wavelength. The sapphire plate intermediates heat flow between crystal and copper. Because thermal conductivity of sapphire is relatively high as ~ 42W/m/K, which is 3 times larger than that of Yb:YAG, the temperature of the sapphire contacting to the copper can be assumed to be nearly equal to T_c. That is, the sapphire can be considered as a heat sink.

Figure 8(a) shows the dependency of the output power P_{out} on the input pump power P_{in} in the two cases. The output power increases nearly linearly in both cases and no apparent saturation phenomenon, below P_{in} ~ 4.0 W, was observable. The slope efficiencies in both cases were higher than for the case of Fig. 4(a). The improved output power performance must be due to the considerably reduced temperature rise in the face cooling cases. It is notable that case B showed slightly higher output power than case A. Because the intensity of the pump beam decreases rapidly by absorption during propagation through the crystal, the input face of the crystal should be hotter than the output face in Fig. 4(a). The sapphire contacting hotter face will remove more efficiently the generated heat than the other case, resulting in the better output performance of case B in Fig. 8(a). In case B, the maximum P_{out} was measured

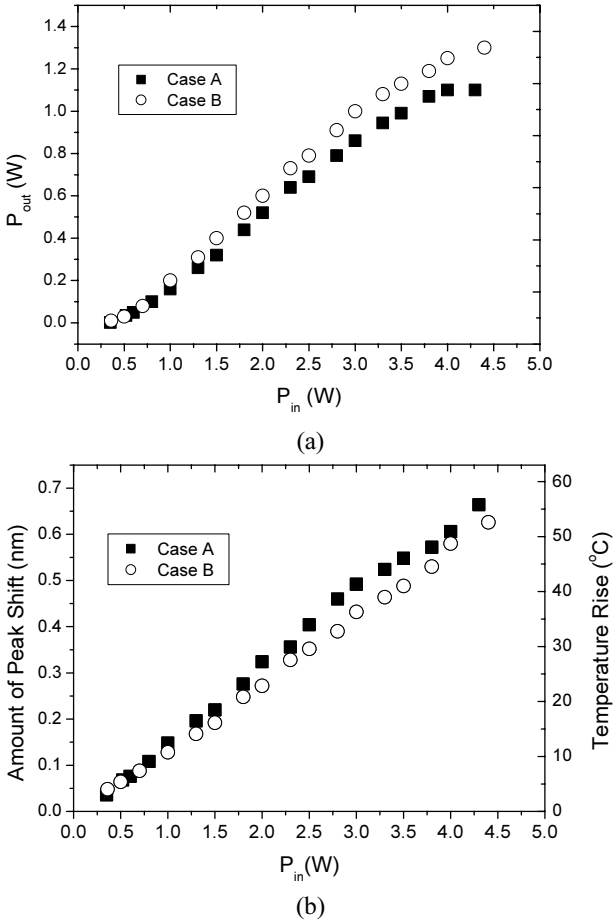

FIG. 8. (a) Dependency of the cw laser output power P_{out} on P_{in} in the face cooling geometry. (b) Dependency of amount of peak shift $\Delta\lambda$ and corresponding temperature rise in the face cooling geometry.

1.3 W, which is about 2 times larger than that in Fig. 2.

In case of Fig. 4(a), the thin crystal is free to expand along both directions so that the axial stress was assumed to be 0. In the face cooling case of Fig. 7, the crystal is also free to expand along one direction so that the axial stress can be also approximated to be 0. As proved by Cousins, PSA is valid in the one-face cooling configuration in the limit of small aspect ratio [18]. Therefore, the relation of Eq. (2) can be also applicable in the face cooling cases in order to obtain the temperature rise.

In order to derive the temperature rise, the amount of peak shift $\Delta\lambda$ was measured by using the spectral analysis procedure used in Fig. 5. Figure 8(b) shows the dependency of $\Delta\lambda$ in both face cooling cases. The temperature rise calibrated by the same SL_{eff} = 0.0119 nm/°C was also shown in Fig. 8(b). The temperature rise in case A was slightly higher than the case B in whole range of P_{in}. This must be because input face cooling is slightly more efficient than the output face cooling, as mentioned. Nevertheless, it can be concluded that the face cooling configuration has similar cooling capacity regardless of the location of the

sapphire plate. The input power corresponding to the temperature rise ~ 45°C, which was the deviation point of the output power in Fig. 2, was around 4.0 W in the face cooling case. Therefore, beginning part of the output saturation curve can be seen in Fig. 8(a) around P_{in} ~ 4.0 W.

The maximum temperature rise in Fig. 8(b) was about 55°C at P_{in} = 4.3 W, which is smaller than the maximum one of 83°C at P_{in} = 3.3 W in Fig. 6(b). Comparison of temperature rises with same P_{in} is meaningful to evaluate the cooling capacity between edge-cooling and face cooled cases. For instance, the temperature rise in case B of Fig. 8(b) was only 37°C at P_{in} = 3.0 W, which is nearly half of 68°C at P_{in} = 3.0 W in Fig. 6(b). The considerable reduction of the temperature rise in Fig. 8(b) should be due to the effective heat removal of the face cooling configuration.

VI. CONCLUSION

We measured temperature rise of an end-pumped monolithic Yb:YAG crystal by using a previous temperature measurement scheme, in which the pumping power level was scaled up to ~ 4 W. Preferential cooling geometry investigated here was the previous PSA valid one where the crystal was sandwiched by copper plates with a central hole. The temperature rise was derived from the lasing spectrum by analyzing the red shift of each lasing peak. Operation properties, such as output power and output beam radius were also investigated. The output power, beam radius, and peak shift showed deviating behaviors around the common input power of ~ 2.3 W, which corresponded to the temperature rise of ~ 45°C. Above this deviation point, the output power showed saturation behavior, the beam size increased rapidly, and the change of the peak shift became steeper due to poor spatial overlapping and increased fractional thermal load. Through the comparison with the previous work, we could conclude that the temperature rise was roughly proportional to the absorbed pump power regardless of the pumping level and pump beam size. PSA valid face cooling geometry was also investigated, in which input or output face of the crystal was contacted with a sapphire plate having high thermal conductivity. The temperature rise was considerably reduced and the laser efficiency was fairly improved in both cases due to the efficient heat removal through the crystal-sapphire interface.

ACKNOWLEDGMENT

This work was supported by the Leading Foreign Research Institute Recruitment program (NRF Grant Number: 2010-00761) funded by the Republic of Korea's Ministry of Science, ICT and Future Planning in the Republic of Korea.

REFERENCES

1. P. Lacovara, H. K. Choi, C. A. Wang, R. L. Aggarwal, and T. Y. Fan, "Room-temperature diode-pumped Yb:YAG laser," Opt. Lett. **16**, 1089-1091 (1991).
2. H. W. Bruesselbach, D. S. Sumida, R. A. Reeder, and R. W. Byren, "Low-heat high-power scaling using InGaAs-diode-pumped Yb:YAG lasers," IEEE J. Sel. Top. Quantum Electron. **3**, 105-116 (1997).
3. P. Yang, P. Deng, and Z. Yin, "Concentration quenching in Yb:YAG," J. Lumin. **97**, 51-54 (2002).
4. J. M. Serres, V. Jambunathan, X. Mateos, P. Loiko, A. Lucianetti, T. Mocek, K. Yumashev, V. Petrov, U. Griebner, M. Aguiló, and F. Díaz, "Graphene Q-switched compact Yb:YAG laser," IEEE Photon. J. **7**, 1503307 (2015).
5. T. Taira, W. M. Tulloch, and R. L. Byer, "Modeling of quasi-three-level lasers and operation of cw Yb:YAG lasers," Appl. Opt. **36**, 1867-1874 (1997).
6. K. Contag, M. Karszewski, C. Stewen, A. Giesen, and H. Hügel, "Theoretical modelling and experimental investigations of the diode-pumped thin-disk Yb:YAG laser," Quantum Electron. **29**, 697-703 (1999).
7. F. D. Patel, E. C. Honea, J. Speth, S. A. Payne, R. Hutcheson, and R. Equall, "Laser demonstration of $Yb_3Al_5O_{12}$ (YbAG) and materials properties of highly doped Yb:YAG," IEEE J. Quantum Electron. **37**, 135-144 (2001).
8. E. Innerhofer, T. Südmeyer, F. Brunner, R. Häring, A. Aschwanden, R. Paschotta, C. Hönninger, M. Kumkar, and U. Keller, "60-W average power in 810-fs pulses from a thin-disk Yb:YAG laser," Opt. Lett. **28**, 367-369 (2003).
9. O. Pronin, J. Brons, C. Grasse, V. Pervak, G. Boehm, M. C. Amann, V. L. Kalashnikov, A. Apolonski, and F. Krausz, "High-power 200 fs Kerr-lens mode-locked Yb:YAG thin-disk oscillator," Opt. Lett. **36**, 4746-4748 (2011).
10. H. Z. Cao, F. J. Liu, H. M. Tan, H. Y. Peng, M. H. Zhang, Y. Q. Chen, B. Zhang, B. L. Chen, and C. J. Wang, "Laser diode end-pumped Yb:YAG/LBO green laser," Laser Physics 1**9**, 919-922 (2009).
11. S. Chénais, S. Forget, F. Druon, F. Balembois, and P. Georges, "Direct and absolute temperature mapping and heat transfer measurements in diode-end-pumped Yb:YAG," Appl. Phys. B **79**, 221-224 (2004).
12. J. Petit, B. Viana, and Ph. Goldner, "Internal temperature measurement of an ytterbium doped material under laser operation," Opt. Express **19**, 1138-1146 (2011).
13. H. J. Moon, C. Lim, G. H. Kim, and U. Kang, "Study of operation dynamics for crystal temperature measurement in a diode end-pumped monolithic Yb:YAG laser," Opt. Express **21**, 31506-31520 (2013).
14. J. T. Verdeyen, *Laser Electronics* (Prentice-Hall, New Jersey, USA, 1995).
15. R. Weber, B. Neuenschwander, and H. P. Weber, "Thermal effects in solid-state laser materials," Opt. Materials **11**, 245-254 (1999).
16. T. Y. Fan, "Heat generation in Nd:YAG and Yb:YAG," IEEE J. Quantum Electron. **29**, 1457-1459 (1993).
17. S. Chénais, F. Druon, S. Forget, F. Balembois, and P. Georges, "On thermal effects in solid-state lasers: The case of ytterbium-doped materials," Prog. Quantum Electron. **30**,

89-153 (2006).
18. A. K. Cousins, "Temperature and thermal stress scaling in finite-length end-pumped laser rods," IEEE J. Quantum Electron. **28**, 1057-1069 (1992).
19. S. Chénais, F. Balembois, F. Druon, G. Lucas-Leclin, and P. Georges, "Thermal lensing in diode-pumped ytterbium lasers- Part II: Evaluation of quantum efficiencies and thermo-optic coefficients," IEEE J. Quantum Electron. **40**, 1235-1243 (2004).
20. A. Giesen, H. Hügel, A. Voss, K. Wittig, U. Brauch, and H. Opower, "Scalable concept for diode-pumped high power solid-state lasers," Appl. Phys. B **58**, 365-372 (1994).
21. S. Tokita, J. Kawanaka, M. Fujita, T. Kawashima, and Y. Izawa, "Sapphire-conductive end-cooling of high power cryogenic Yb:YAG lasers," Appl. Phys. B **80**, 635-638 (2005).
22. M. S. N. Kazi, *An Overview of Heat Transfer Phenomena* (Intech, http://dx.doi.org/10.5772/2623, 2012) Chapter 12.
23. A. Giesen, "Thin disk lasers power scalability and beam quality," Laser Technik J. **2**, 42-45 (2005).